Article

Not peer-reviewed version

LPS-Induced Systemic Inflammation Affects the Dynamic Interactions of Astrocytes and Microglia with the Vasculature of the Mouse Brain Cortex

Evangelia Xingi , Paraskevi N. N Koutsoudaki , Irini Thanou , Minh-Son Phan , Maria Margariti , Anja Scheller , Jean-Yves Tinevez , Frank Kirchhoff , Dimitra Thomaidou *

Posted Date: 30 March 2023

doi: 10.20944/preprints202303.0525.v1

Keywords: astrocytes; microglia; 2-photon imaging; NVU; LPS; blood vessels; AQP4

Article

LPS-Induced Systemic Inflammation Affects the Dynamic Interactions of Astrocytes and Microglia with the Vasculature of the Mouse Brain Cortex

Evangelia Xingi [1,§], Paraskevi N. Koutsoudaki. [2,#,§], Irini Thanou [2], Minh-Son Phan [3], Maria Margariti [2], Anja Scheller [4], Jean-Yves Tinevez [3], Frank Kirchhoff [4] and Dimitra Thomaidou [1,2,*]

[1] Light Microscopy Unit, Hellenic Pasteur Institute, Athens, Greece
[2] Neural Stem Cells and Neuroimaging Group, Department of Neurobiology, Hellenic Pasteur Institute, Athens, Greece
[3] Institut Pasteur, Université de Paris, Image Analysis Hub, F-75015 Paris, France
[4] Molecular Physiology, Center for Integrative Physiology and Molecular Medicine (CIPMM), University of Saarland, 66421, Homburg, Germany
[#] Present address: Molecular Carcinogenesis Group, Department of Histology and Embryology, Medical School, National and Kapodistrian University of Athens, Athens, Greece
[§] These authors contributed equally.
[*] Correspondence: thomaidou@pasteur.gr

Abstract: The Neurovascular Unit (NVU), comprised of glia (astrocytes, oligodendrocytes, microglia), neurons, pericytes and endothelial cells, is a dynamic interface ensuring physiological functioning of the central nervous system (CNS), that gets affected and contributes to the pathology of several neurodegenerative diseases. Neuroinflammation is a common feature of neurodegenerative diseases and is primarily related to the activation state of perivascular microglia and astrocytes, which constitute two of its major cellular components. Our studies focus on monitoring in real time the morphological changes of perivascular astrocytes and microglia, as well as their dynamic interactions with the brain vasculature, under physiological conditions and following systemic neuroinflammation triggering both microgliosis and astrogliosis. To this end, we performed 2-photon laser scanning microscopy (2P-LSM) for intravital imaging of the cortex of transgenic mice visualizing the dynamics of microglia and astroglia following neuroinflammation induced by systemic administration of the endotoxin lipopolysaccharide (LPS). Our results indicate that following neuroinflammation the end-feet of activated perivascular astrocytes lose their close proximity and physiological crosstalk with vasculature, an event that most possibly contributes to a loss of blood-brain-barrier (BBB) integrity. At the same time, microglial cells get activated with more frequent contacts of the blood vessels. These dynamic responses of perivascular astrocytes and microglial are peaking at 4 days following LPS administration, however they still persist at a lower level 8 days after LPS, revealing incomplete reversal of inflammation affecting the glial properties and interactions with the NVU.

Keywords: astrocytes; microglia; 2-photon imaging; NVU; LPS; blood vessels; AQP4

1. Introduction

Neuroinflammation plays an important role in the progression of a variety of chronic neurological/neurodegenerative diseases. A common inflammatory feature of neurodegenerative diseases is the activation of microglia and astrocytes, as well as the presence of proinflammatory cytokines and altered composition of gliotransmitters secreted as part of the intercellular crosstalk [1,2].

 doi:10.20944/preprints202303.0525.v1

Astrocytes play a major role in CNS blood flow regulation and exchange of nutrients and other functional signals between the peripheral blood and brain parenchyma. This regulation is achieved by extension of their specialized processes called endfeet to the blood vessel walls. Astrocytic endfeet that enwrap the vasculature are in physical contact with the basal lamina component of the vessel wall, forming, together with perivascular pericytes and neurons a dynamic interface characterized as the neurovascular unit (NVU) [2]. Under physiological conditions, perivascular astrocyte endfeet express molecules that maintain the integrity of the blood-brain barrier (BBB), including enzymatic and transporter proteins, the most important one being the water channel Aquaporin 4 (AQP4) [3]. Disruptions of the association of astrocytic endfeet to brain vasculature result in decreased coverage of vessel walls and may contribute to loss of BBB integrity and functional impairment, which has been reported to occur during progression of neurodegenerative diseases. A number of CNS diseases, such as multiple sclerosis [4], major depressive disorder [5] and ischemia [6], are marked by retraction or separation of astrocytic endfeet from blood vessels, a phenotype often accompanied by vascular deficits indicative of BBB breakdown, such as altered BBB permeability or elevated CSF-to-serum albumin ratio. Microglial cells located in close proximity to the NVU on the other hand appear to get also implicated in NVU integrity and homeostasis, as they have been shown to rapidly repair the BBB following acute vessel injury [7].

Despite many indications linking NVU dynamics to glial cells inflammatory responses during progression of CNS diseases, there are few data monitoring the dynamic interactions of astrocytes and microglia with brain vasculature following systemic inflammation which triggers both microgliosis and astrogliosis. These dynamic interactions can be captured by in vivo imaging, which allows study of cellular responses to neuroinflammation in the living brain in real time (Helmchen and Denk 2005; Davalos et al. 2008). To this end, we used 2-photon laser scanning microscopy (2P-LSM) intravital imaging of the cortex of transgenic mice, to visualize and quantify the dynamic interactions of microglia and astroglia with blood vessels after neuroinflammation evoked by systemic administration of the bacterial wall endotoxin lipopolysaccharide (LPS). LPS is considered a potent activator of neuroinflammation after its peripheral administration and has been extensively used in AD, PD, ALS and HD animal models [10]. Our data reveal that following LPS administration, hypertrophy of the cell body of astrocytes - and microglia, which constitutes a main feature of glial cell activation takes place. At the same time, endfeet of activated perivascular astrocytes lose their proximity to the vasculature, while activated microglial cells exhibit an opposite response pattern, as the extent of contact between their processes/ cell bodies and blood vessels increases. These dynamic responses of perivascular astrocytes and microglia are peaking 4 days following LPS administration and still persist at a lower level at the longer time point of 8 days, revealing the lasting effect of inflammation on the cellular properties and interactions at the NVU.

2. Materials and Methods

Experimental Animals

To visualize the morphology of microglia with 2-photon microscopy we used heterozygous Cx3cr1-EGFP transgenic mice of both sexes expressing enhanced green fluorescent protein (EGFP) knocked into the Cx3cr1 locus, which is specific for microglia, macrophages, and monocytes [11] in C57BL/6J background. To visualize the morphology of astrocytes we used hGFAP-ECFP transgenic mice expressing enhanced cyan fluorescent protein (ECFP) under the control of the human GFAP promoter which is specific for astrocytes in an FVB/N genetic background [12]. For confocal microscopy experiments we used 9-11 weeks old wild type, both male and female C57BL/6J mice, n=3-4 for each condition.

Cranial window surgery

Cranial window surgery was performed in 6-8 week old Cx3cr1-EGFP or hGFAP-ECFP transgenic mice. Following anesthesia with ketamine (100mg/kg), xylazine (15 mg/kg) and acepromazine (2,5 mg/kg) the skull was exposed and cleaned. A circular (~3 mm in diameter)

 doi:10.20944/preprints202303.0525.v1

craniotomy was performed with a driller over the somatosensory cortex. The bone was gently lifted, ACSF (Tocris) was applied to clean and remove dural bleedings and a glass window (3 mm diameter) was placed over the brain surface. A custom-made head bar was positioned over the craniotomy and was firmly affixed to the skull with cyanoacrylate glue and dental cement (Unifast Trad). The edges of the cranial window were also sealed with dental cement. Imaging sessions of living animals started 3 weeks after cranial window surgery (when mice were aged 9-11 weeks old), to allow inflammation resulting from the surgical procedure to resolve.

2-photon imaging

For each imaging time-point Cx3cr1-EGFP or hGFAP-ECFP transgenic mice were anesthetized as described in the previous paragraph and the vascular marker Rhodamine B dextran (M.W. 70 KDa, Sigma) was intravenously injected (3%, 50 µl). Their temperature was monitored and kept at 37°C using a heating pad during the entire imaging sessions and until their recovery from anesthesia. Animals were head restrained at the stage of a Leica TCS-SP5 2-photon microscope equipped with a 25x water-injection objective (NA 0.9) and a Ti-sapphire laser Mai Tai DeepSee (Spectra Physics) tuned to an excitation wavelength of 900 nm. Imaging was performed 100 µm below the dura in the somatosensory cortex. Image z-stacks were typically 1024 x 1024 pixels with voxel size of 0.144 (x) x 0.144 (y) x 0.988 (z) µm acquired for all samples. A 560 nm dichroic mirror was used to separate 525/50 nm (green channel for EGFP fluorescence detection) or 483/32 nm (cyan channel for ECFP fluorescence detection) and 585/40 nm (red channel for Rhodamine B dextran fluorescence detection) emission filters and fluorescence was collected using NDD detectors.

Systemic LPS administration

LPS (Lipopolysaccharides from Escherichia coli serotype 055:B5; Sigma) was administered to induce systemic inflammation. For 2-photon in vivo imaging experiments of mouse brains, 9-11 weeks old, Cx3cr1-EGFP (n=5) or hGFAP-ECFP (n=5) transgenic animals with cranial window firmly attached to the skull were treated with LPS with the following scheme: Untreated mice had a 2-photon imaging session through their cranial window and the next day two doses of LPS (5 mg/kg, i.p.) were administered with a time interval of 24 hours (day-1 and day 0), as-shown in Figure 2A. Two more 2-photon imaging sessions were performed for each animal at time points LPS day 4 and LPS day 8 after the last LPS injection.

For confocal imaging experiments adult C57BL/6J mice (9-11 weeks old) were injected with the same scheme of LPS as previously and sacrificed at 1 (LPS 1 day, n=3), 4 (LPS 4 days, n=4) and 8 days (LPS 8 days, n=4) after the second LPS injection (p.i). An untreated group of animals of the same age were used as controls (n=4).

Immunohistochemistry

Mice were deeply anaesthetized by isoflurane inhalation, and perfused with 4% paraformaldehyde (PFA) via the left cardiac ventricle. Brains were removed, post-fixed in 4% PFA overnight, and then cryoprotected in 20% sucrose overnight. After cryoprotection brains were frozen in OCT compound and cut into 20 µm-thick coronal sections on a cryostat (Leica CM1900, Nussloch, Germany), collected on silane-coated slides and stored at −20°C until further processing.

For immunofluorescence experiments, sections were left for 15 min at room temperature, washed in PBS, and blocked with 5% normal donkey serum (Merck-Millipore, Massachusetts, USA) in PBT (0.5% Triton X-100/PBS) for 1 h. Incubation with primary antibodies was performed overnight at 4°C. After PBS wash, sections were subsequently incubated with secondary antibodies in PBS at room temperature (RT) for 3 h. Finally, sections were washed and embedded with Mowiol (Calbiochem, California, USA).

The following antibodies were used for staining: for astrocytes rabbit anti-GFAP (1:500, Dako, Z0334), mouse anti-GFAP (1:200, Sigma G-3893), for vessels goat anti-CD31 (1:200, R&D Systems, AF3628), for astrocyte endfeet mouse anti-AQP4 (1:200, Santa Cruz Biotechnology, sc-32739), for

 doi:10.20944/preprints202303.0525.v1

microglia rabbit anti-Iba1 (1: 500, Wako chemicals, 019-19741). Secondary antibodies used were conjugated with AlexaFluor 488 (green), 546 (red), 647 (1:600, all from Biotium, USA) and Hoechst (1: 600) for nuclei staining.

Images were acquired using a Leica TCS-SP5 confocal microscope (LEICA Microsystems, Germany) with a 40x objective (NA 1.3) using a pixel size of 0.361 x 0.361 x 1 µm and a Leica TCS-SP8 confocal microscope with a 40x objective (NA 1.3) using a pixel size of 0.284 x 0.284 x 1 µm. Images were typically 1024 x 1024 pixels.

Image analysis

Image analysis was performed with the Fiji software [13], Python Jupyter notebooks [14] and Imaris (v 9.3.1, Bitplane). We provide the Fiji macros and notebooks for the entire image analysis pipeline above and they can be downloaded from the public code hosting website: https://gitlab.pasteur.fr/iah-public/ptrmiad-mimika

To measure cell body volumes of microglia and astrocytes in 2-photon images, we first applied auto-thresholding using Renyi Entropy [15] to segment the cell body. Morphological opening with radii = 5.5 and 2 pixels in x, y and z was then used to exclude the remaining processes from the segmented objects. The touching cell bodies were split using watershed separation in the MorphoLibJ plugin [16]. This tool was used to remove spurious detection by setting a minimum volume of 200 μm^3, a minimum mean intensity of 60 and a maximum flatness of 3.5 for objects.

To measure the contact ratio between microglia, astrocytes and the blood vessels in 2-photon images, we first smoothed the images by a Gaussian filter with sigma = 2 pixels and enhanced the image contrast by saturating pixels with a percentage of 0.7%. The intensity in the blood vessels channel was subtracted to the intensity in the microglia/astrocytes channel to remove the wavelength mixing effect. Microglia, astrocytes and the blood vessels were then segmented by auto-thresholding using the Otsu method [17], and overlapping regions were identified from their masks across z slices, from which we deduced the contact ratio.

Confocal images with Aquaporin 4 contacts of the blood vessels (CD31) were analyzed using Imaris surface-surface contact area XTension. More specifically a primary surface of the CD31 staining and a secondary of the Aquaporin 4 staining were created and the percentage of the new surface contact area relative to the total surface area of the primary surface was estimated using XTension.

Analyses of microglia and astrocytic reactivity were performed as quantification of the areas immunostained positive for Iba1 and GFAP, respectively. Measurements were performed on maximum intensity projections of confocal z stacks of ~30µm using automatic thresholding Default for microglia and MaxEntropy for astrocytes in Fiji.

Statistical analysis

All quantified data are presented as average ± standard error of the mean (SEM). Values from each quantification performed were averaged per animal, and data were assessed using a one-way analysis of variance (ANOVA). When interactions were detected, group comparisons were performed using a two-sample assuming unequal variances test. The level of statistical significance was set at 0.05.

3.1. Results

3.1.1. LPS systemic administration activates perivascular astrocytes and microglia.

To determine the time frame during which perivascular glial cell populations, including microglia and astrocytes, become activated in response to systemically induced inflammation, we administered to 9-11 weeks old C57BL/6J mice 2 daily doses of LPS (5 mg/kg each). Animals were sacrificed 1, 4 and 8 days following the second dose of LPS administration and their brains further proceeded to immunofluorescence labelling. Immunofluorescence analysis of Iba1 and GFAP expression levels in the somatosensory cortical area at all time points revealed that both microglia

 doi:10.20944/preprints202303.0525.v1

and astrocytes exhibited the highest expression of Iba1 and GFAP, respectively, 4 days following LPS administration, indicating the time window of their highest activation **(Figure 1A-D).** More specifically Iba1 and GFAP immunopositive areas (μm²) were measured on maximum intensity projections of brain cortical z stacks as described in Materials and Methods section **(Figure 1 E, F).** Regarding microglia, in control mice Iba1 area was 5421 μm² ± 263 μm² , whereas 1 day post injection (p.i.) of LPS an increase was already evident [7025 μm²± 448 μm²]. Four days p.i. of LPS Iba1 expression further increased [9347 μm²± 171 μm²], while at 8 days p.i. of LPS the Iba1 area decreased [6718 μm²± 244 μm²]. Regarding astrocytes, in control mice GFAP area was 733.8 μm² ± 65.7 μm², whereas 1 day p.i. of LPS 2319 μm² ± 79 μm². At the LPS 4 days p.i. time-point, the GFAP area further increased to 4081 μm²± 13 μm² , while it decreased to 2249 μm²± 149 μm² 8 days p.i. of LPS administration.

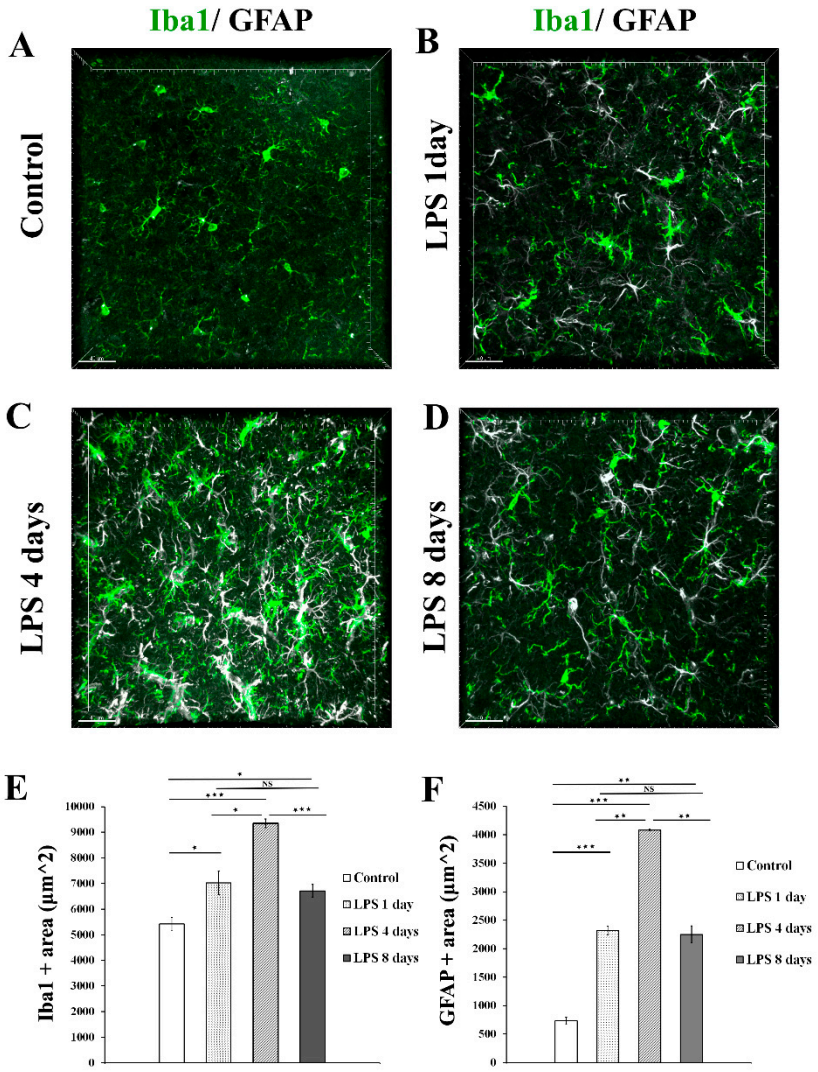

Figure 1. Time course of astrocytes and microglia activation following LPS induced inflammation. **(A-D)** Immunofluorescence staining for microglia (Iba1-green) and astrocytes (GFAP-white) in the cortex of C57BL/6J mice cortical brain slices, showed the highest Iba1 and GFAP expression levels at 4 days after LPS injection. Images were acquired with a Leica TCS SP5 confocal microscope using a 40x objective. (**E-F)** Quantification of Iba1 (E)and GFAP (F) immunopositive area (μm²) in maximum intensity projections in control (n=4), LPS day 1 (n=3), LPS day 4 (n=4) and LPS 8 days (n=4). (E) Control vs LPS 1 day p=0.05, control vs LPS 4 days p=0.00005, LPS 4 days vs LPS 8 days p=0.0003. (F) Control vs LPS 1 day p=0.0001, control vs LPS 4 days p=0.00001, LPS 4 days vs LPS 8 days p=0.006 Scale bar: 40μm.

 doi:10.20944/preprints202303.0525.v1

Following confocal analysis, we established a protocol of 2-photon intravital imaging of the cortex of transgenic mice expressing fluorescently labeled proteins in the microglial or astrocytic cell populations following systemic administration of 2 daily doses of LPS, to monitor in real time the dynamic response of microglia and astrocytes to systemically induced inflammation **(Figure 2A)**.To this end, Cx3cr1-EGFP and hGFAP-ECFP transgenic mice were subjected to a surgical operation for establishment of a cranial window and 3 weeks later they were anaesthetized and their cortical microglia and astrocytes were imaged by 2-photon microscopy under control conditions. For each of the next two days (day -1 and day 0) the same mice received 5mg/kg of LPS and were imaged at days 4 and 8 after the second dose of LPS injection. The acquired image z-stacks were analyzed using Fiji-based custom-made macros that allowed quantification of microglial and astrocytic 3D cell body volume as well as the extent of contact with blood vessels in multiple image data sets.

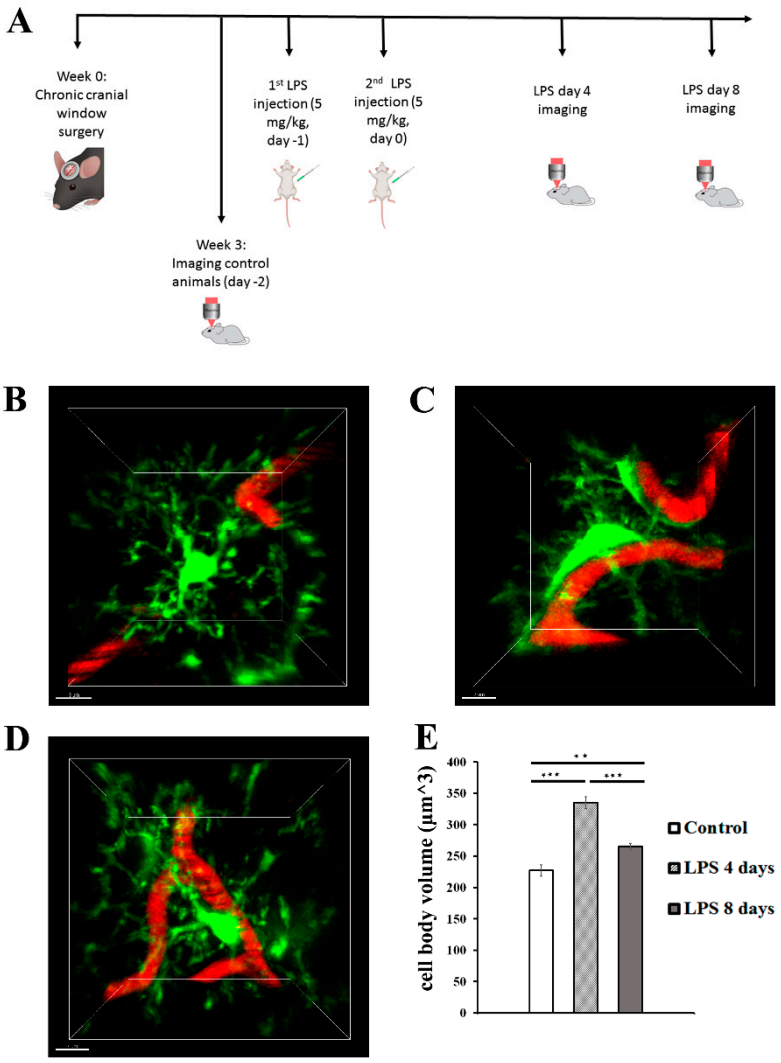

Figure 2. LPS-induced inflammation results in changes in microglia cell body volume and morphology. (A) Protocol of brain intravital 2-photon imaging following LPS systemic administration. At week 0 a cranial window surgery was performed in 6-8 week old Cx3xr1-EGFP or hGFAP-ECFP transgenic mice. Three weeks after surgery, imaging experiments of untreated control animals were performed, in order to eliminate inflammation caused by the cranial window surgery. The next two sequential days mice were injected with LPS (5 mg/kg) and imaging was performed at 4 days and 8 days after the second dose (LPS day 4 and LPS day 8 time points). (B-D) Two-photon magnified images of Cx3cr1-EGFP microglial cells (green) associated with blood vessels marked with Rhodamine B dextran (red). B) An untreated control animal, imaged 3 weeks after cranial window surgery. C) The same animal imaged 4 days after LPS administration D) The same animal imaged 8

 doi:10.20944/preprints202303.0525.v1

days after LPS administration. E) Bar graph presents quantification of the mean volume of the microglial cell soma in the three time points. Multiple images from Cx3cr1-EGFP mice (n=5) were analyzed. **P < 0.01, and ***P < 0.001. Scale bar: 7 μm.

2-photon imaging at 4 days p.i. of LPS revealed the microglial cell response to LPS-inflammation in greater detail, with microglia exhibiting morphological alterations indicative of an activated state, by becoming hypertrophic and acquiring a less ramified amoeboid-like elongated morphology (**Figure 2B-D**). More specifically data obtained from 5 Cx3cr1-EGFP mice showed a significant increase of the cell body volume by 47. 6% (from 226.9 ± 8.9μm^3 to 334.9 ± 9.7 μm^3) 4 days p.i. of LPS as compared to control conditions (**Figure 2B-C, E**). At the same time microglia cell bodies were observed in close proximity to blood vessels **(Figure 2B, C, D; Video S1** for LPS day 0 and **Video S2** for LPS day 4**)**. Microglia activation was lower but persistent at 8 days p.i. of LPS, as indicated by the statistically significant decrease of microglial cell body volume (265.4± 4.5 μm^3) in comparison to 4 days p.i. of LPS **(Figure 2B-E)**; which however didn't appear to return to control levels, as cell body volume was still increased by 16.9% as compared to control cell body volume **(Figure 2E; Video S3).** We also observed a relative restoration of ramified morphology and lower extent of contact with blood vessels as compared to 4 days p.i, **(Figure 2C, D; Video S2)**.

LPS administration also induced a significant increase in astrocytic cell body volume 4 days p.i. indicative of astrocytic activation, which was accompanied by retraction of astrocytic endfeet from blood vessels **(Figure 3A, B, D; Video S4** for LPS day 0**, Video S5** for LPS day 4), with data obtained from 5 hGFAP-ECFP transgenic mice showing a 54.5% increase of the cell body volume (from 704.8 ± 45.5 μm^3 to 1089 ± 66.8 μm^3). Astrocytic cell body volume significantly decreased by 22.6% 8 days p.i of LPS (842.8 ± 69 μm^3), as compared to 4 days p.i of LPS, and becoming not significantly higher than in control animals **(Figure 3C, D; Video S6)**.

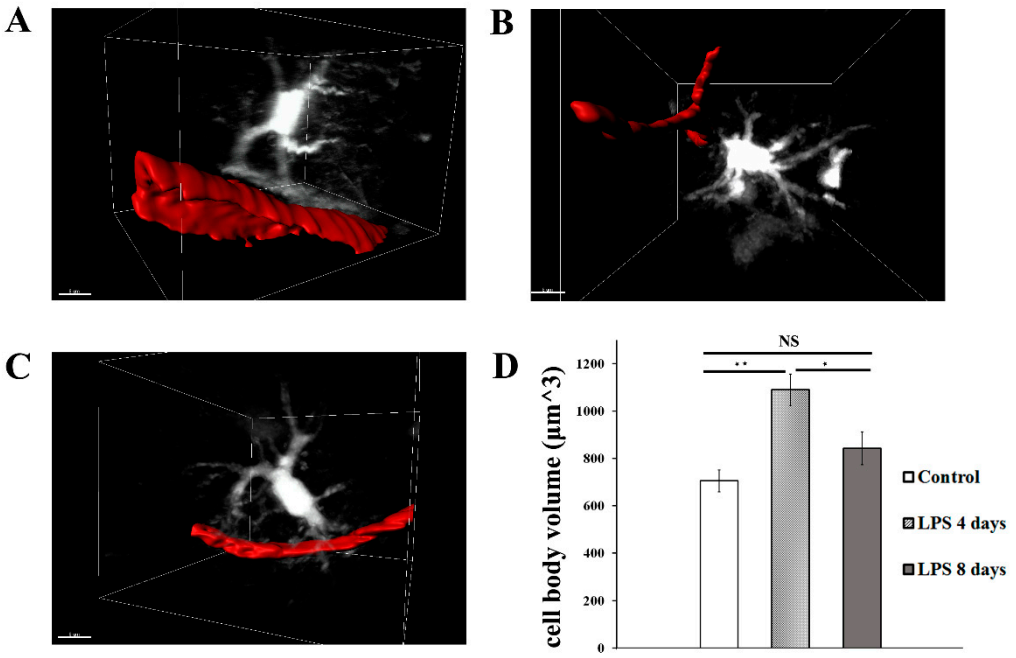

Figure 3. LPS induced inflammation results in changes in astrocytes cell volume and morphology. 2-photon magnified images of hGFAP-ECFP astrocytes (white) associated with blood vessels marked with Rhodamine B dextran (red). For visualization purposes blood vessels are highlighted with a surface created with Imaris. A) An untreated control animal, imaged 3 weeks after cranial window surgery. B) the same animal imaged 4 days after LPS administration. C) the same animal imaged 8 days after LPS administration D) Bar graph presents quantification of the mean volume of the astrocytic cell soma in three time points. Multiple images from hGFAP-ECFP mice (n=5) were analyzed. *P < 0.05, **P < 0.01, NS not significant. Scale bar 8 μm.

 doi:10.20944/preprints202303.0525.v1

3.1.2. Astrocytic endfeet reduce their close proximity to blood vessels following LPS-induced neuroinflammation

Analysis of 3D intravital imaging data derived from Cx3cr1-EGFP and hGFAP-ECFP mice indicated that LPS systemic administration induced dynamic changes in the contact of both perivascular microglia and astrocytes with the blood vessels. To quantify in real time the extent of contact of each of the two cell populations with the cortical vasculature, we developed a Fiji macro to measure contact volume (of either astrocytes or microglia) to blood vessels volume in a batch mode in multiple image data-sets. Measurements of astrocytes-vessels contact volume relatively to total volume of vessels (illustrated in yellow) in hGFAP-ECFP mice **(Figure 4A-C)** point to a significant decrease in the contact of astrocytes to the vasculature at 4 days p.i. of LPS by 32.9% as compared to the control condition, confirming our original observation, a phenomenon which was not significantly reversed 8 days p.i. of LPS **(Figure 4D).**

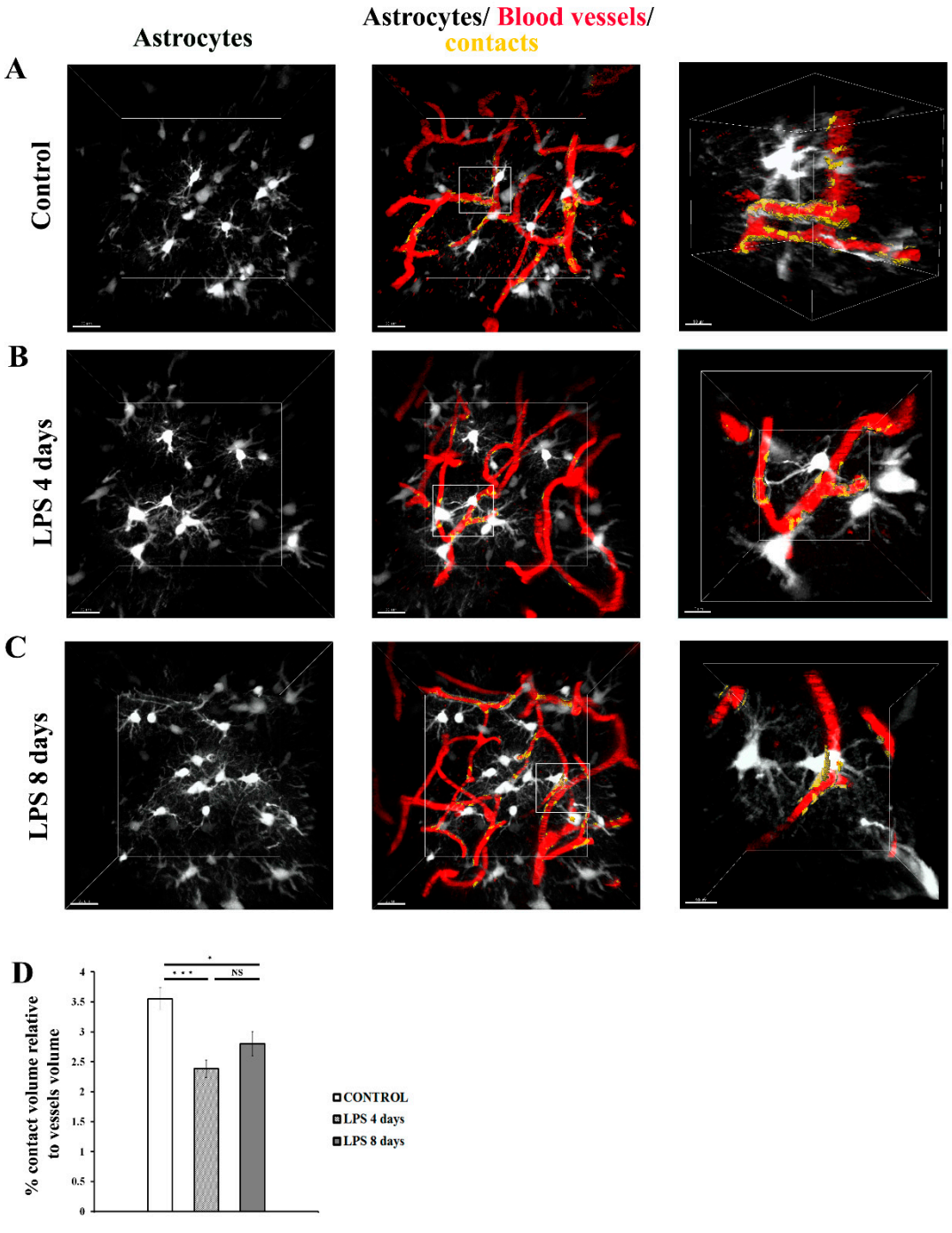

 doi:10.20944/preprints202303.0525.v1

Figure 4. Dynamic changes in the contact of astrocytic endfeet with blood vessels following LPS-induced inflammation. 2-photon image z stacks from a single hGFAP-ECFP transgenic mouse demonstrate astrocyte retraction from cerebral vessels during systemic inflammation induced by two doses of LPS (5mg/kg each). The left column shows astrocytes depicted in white, the middle column shows astrocytes, blood vessels (in red) and their contacts (in yellow). The right column shows magnified images of the region indicated in the main panel (scale bar 10 μm). A) An untreated control animal, imaged 3 weeks after cranial window surgery. B) the same animal imaged 4 days after LPS administration. C) the same animal imaged 8 days after LPS administration. Scale bar, 20 μm. D) Bar graph presents quantification of the percentage of the contact volume (between astrocytes and the vessels) relative to the vessels volume (n=5). Quantification was performed using a customized Fiji macro, as described in Materials and Methods section. NS not significant. *P < 0.05, ***P < 0.001. Visualization of contact areas was performed using Imaris software.

To further explore this finding, which is indicative of a less efficient enwrapping of blood vessels by astrocytic endfeet following LPS administration, we investigated the localization pattern of the water channel AQP4, known to be localized in astrocytic endfeet under physiological conditions [18]. Immunohistochemical labelling of the cortex of C57BL/6J mice using antibodies against AQP4 and CD31 to label blood vessels, revealed that in control animals the percentage of the surface contact area between AQP4 and blood vessels, relative to the surface area of blood vessels is 13.2± 0.6 % **(Figure 5A-C).** This value got severely reduced by 54% 4 days p.i. of LPS and remained low 8 days p.i LPS injection [control: 13.2% ± 0.6%, 4 days LPS: 6.06% ± 0.6%, 8 days LPS: 7.48% ± 0.5%], **(Figure 5D**). These findings further corroborated reduced physical contact between astrocytes and the blood vessel surface as found by 2-photon imaging experiments, and jointly indicate a loosening of the enwrapping of blood vessels by astrocytic endfeet following LPS administration. In parallel with reduced AQP4+ endfeet physical contact with vessels, a significant reduction in overall AQP4 expression levels was evident both at 4 and 8 days p.i. of LPS as compared to control conditions (**Figure 5E).** AQP4 volume in control: 6480 ± 408 μm^3, LPS 4 days: 2875 ± 385 μm^3, LPS 8 days: 3772 ± 444 μm^3), indicating that that of LPS-induced inflammation results in reduction of both diffused and polarized astrocytic endfeet AQP4 expression.

3.1.3. Activated microglia processes enwrap blood vessels following LPS-induced neuroinflammation

To estimate the dynamic interactions of microglia with blood vessels in our model, we measured the percentage of the microglia-vessels contact volume relatively to the total volume of vessels (illustrated in white) in Cx3cr1-EGFP transgenic mice **(Figure 6A-C)**. Our data indicated that in contrast to astrocyte-vasculature interactions, activated microglial cells exhibited a significant increase in their contacts with the vasculature 4 days p.i. of LPS in comparison to control animals (3.29 ± 0.15% vs 1.82 ± 0.15%, **Figure 6D**). This increase in microglia-vessel contact volume was partially reversed -in LPS day 8 (2.53± 0.13%), however without returning to control levels.

 doi:10.20944/preprints202303.0525.v1

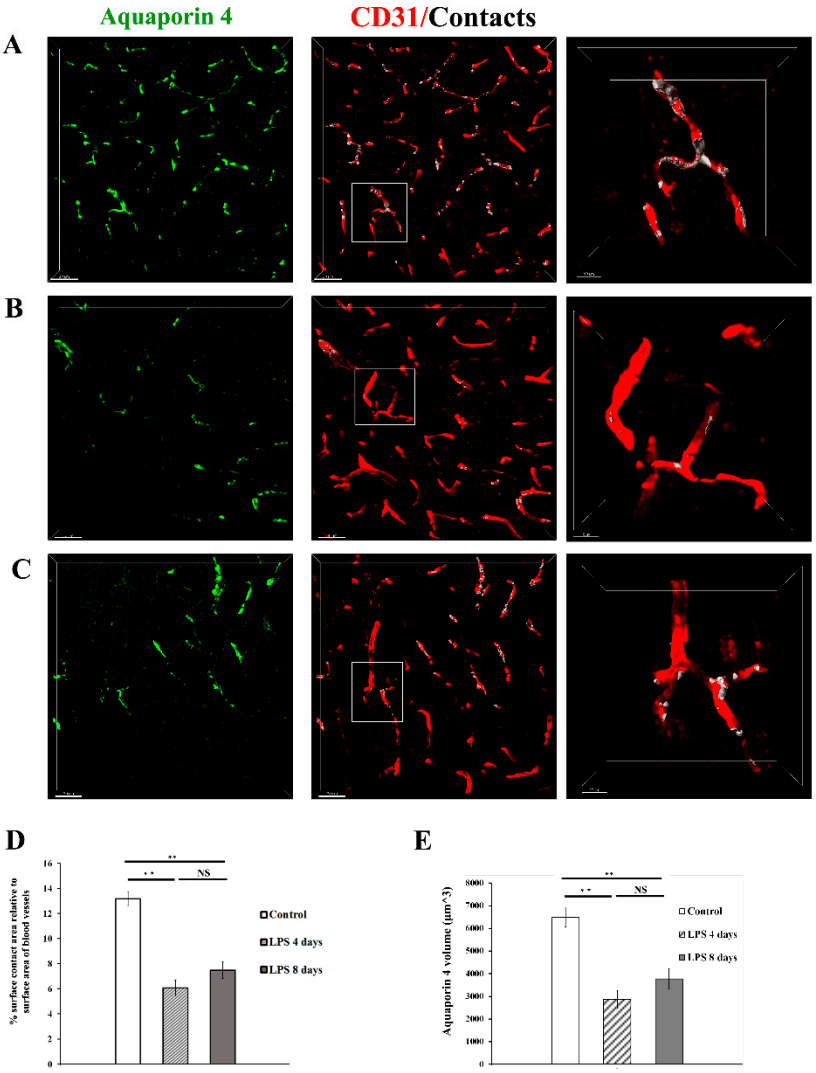

Figure 5. Expression of AQP4 in astrocytic endfeet following LPS-induced inflammation. Confocal images from C57BL/6J mice (9-11 weeks old) brain slices acquired with 40x objective using a Leica TCS SP8 confocal microscope. The brain slices were immunolabelled for AQP4 (green) showing astrocytic endfeet, and CD31 (red) showing blood vessels. Scale bar, 30 µm. Contact areas between astrocytic endfeet and the blood vessels are shown in white colour in the third column. The right column shows magnified images of the region indicated in the main panel (scale bar 10 µm). A) Control animal, which received sterile physiological saline i.p. B) mouse injected with 2 doses of LPS (5 mg/kg, i.p. each) for 2 consecutive days and was sacrificed at LPS day 4 time-point, and C) mouse injected with 2 doses of LPS (5 mg/kg, i.p. each) for 2 consecutive days and was sacrificed at LPS day 8 time point. D) Quantitative analysis of the percentage of the surface contact area (between blood vessels and AQP4) relative to the total surface area of the blood vessels in control (n=3), LPS 4 days (n=3) and LPS 8 days (n=3). **P < 0.01, NS not significant. Analysis was performed using the Imaris surface-surface contact area XTension.E) Quantification of AQP4 total volume (µm3) was measured using Imaris v.9.3.1 surfaces module.

 doi:10.20944/preprints202303.0525.v1

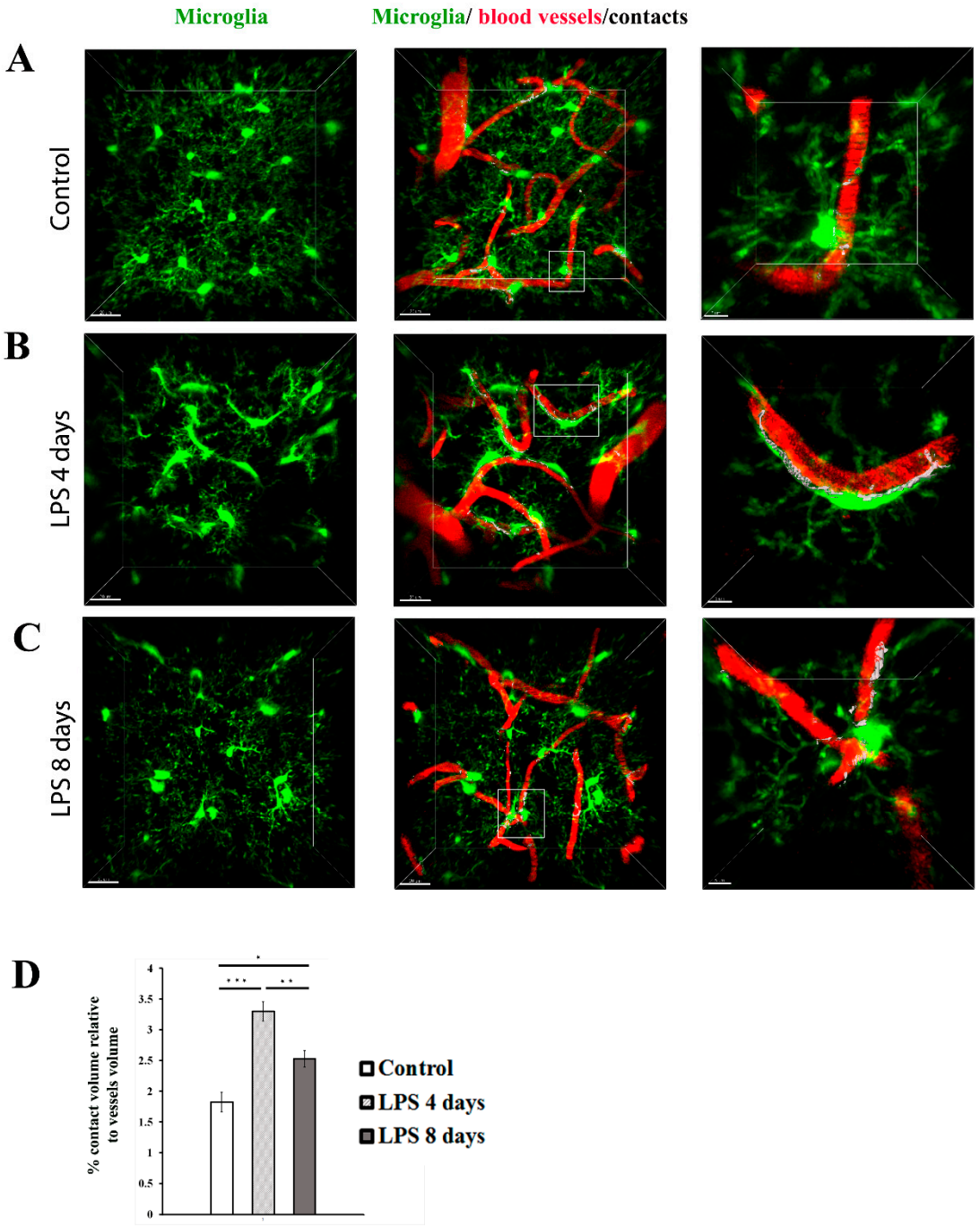

Figure 6. Dynamic changes in the contact of microglia processes with blood vessels following LPS-induced inflammation. 2-photon image z stacks from a single Cx3cr1-EGFP transgenic mouse demonstrate microglia migration to cerebral vessels during systemic inflammation induced by two doses of LPS (5 mg/kg each). Microglia cells are depicted in green color, blood vessels in red and their contacts in white. Close-ups of the merged images are shown in the right panels. (scale bar 5 μm). A) An untreated control animal, imaged 3 weeks after cranial window surgery. B) The same animal imaged 4 days after LPS administration. C) The same animal imaged 8 days after LPS administration. Scale bar, 20 μm. Visualization was performed using Imaris software. D) Bar graph presenting quantification of the percentage of the contact volume relative to the vessels volume (n=4). *P < 0.05, **P < 0.01, and ***P < 0.001.

 doi:10.20944/preprints202303.0525.v1

4. Discussion

Neuroinflammation is a common pathological event observed in many different brain diseases, triggering among others activation of microglia and astroglia which acquire distinct inflammatory phenotypes [19,20]. Following neuroinflammation an extensive crosstalk occurs between reactive microglia and astrocytes, with reactive astrocytes acquiring a neurotoxic phenotype induced by cytokines released by microglia [21]. Neuroinflammation has been also associated with BBB dysfunction, while recent single cell transcriptomic studies have revealed that a sub-population of reactive astrocytes following LPS-induced systemic inflammation differentially expresses genes associated with brain vasculature, highlighting the role of perivascular astrocytes in inflammatory response [20]. Although there are indications that disruption of the association of astrocytic endfeet with brain vasculature takes place under neuroinflammatory / neurodegenerative conditions, the data concerning the extent of contribution of astrocytic endfoot coverage on BBB integrity are still contradictory [22–24]. Additionally, there is scant evidence concerning the position of microglia processes and cell bodies relatively to blood vessels following neuroinflammation and their contribution to BBB integrity.

In this study we used 2-photon intravital imaging to monitor and quantify in real time the activation state and dynamic interactions of both astrocytes and microglia with the brain vasculature following systemic brain inflammation. Our data reveal that the two glial populations exhibit an opposing pattern of blood vessel coverage, with astrocytes retracting their endfeet from the vasculature at the peak of the inflammatory response, while at the same time microglia processes contact and enwrap blood vessels. This observation implies an active crosstalk of microglia and astrocytes and the possible existence of a compensatory mechanism of reactive microglia to maintain BBB integrity following astrocytic endfeet retraction. This mechanism seems to be in place from early developmental stages, according to findings showing that microglia associate with capillary vasculature in the healthy, developing, and adult brain in areas lacking astrocytic coverage [25]. However, in contrast to astrocytes which maintain their endfeet retracted from blood vessels for a longer period of time, microglia mostly exhibit a more transient response, forming fewer contacts with the vasculature in the later time point examined. Coverage of the blood vessels by microglia seems to temporally follow the duration of LPS administration, that possibly sustains a certain threshold of inflammatory conditions [26]. Our data complement recent findings on the role of microglia following systemic inflammation, which demonstrate a dual role for microglia in BBB permeability following systemic inflammation, by contacting endothelial cells at initial stages of inflammation, and phagocytosing astrocytic endfeet thus impairing BBB function at later stages [26]. They also come in accordance with previous reports showing that microglial cells rapidly repair the BBB following acute vessel injury [7], further supporting the protective role microglia holds in the maintenance of BBB integrity in synergy with astrocytes.

Consistent with the retraction of astrocytic endfeet from blood vessels in response to systemic inflammation, we observed a significant reduction of diffuse AQP4 expression levels, and accompanied by minimal polarized AQP4 localization at the level of blood vessel walls. AQP4 is the predominant water channel in the CNS, expressed primarily in the endfeet of astrocytes [18] and it is responsible for maintaining water and ion homeostasis associated with neuronal activity. Thus, our findings showing reduced presence of AQP4 expression in astrocytic endfeet following neuroinflammation come in accordance with studies linking neuroinflammation and BBB leakage with AQP4 channel dysregulation [27]. Moreover, the involvement of AQP4 in a astrocytic process plasticity [28] give rise to the question of whether AQP4 plays a role in endfeet plasticity and eventually vessel coverage [24]. Our results showing continuation of AQP4 expression dysregulation at the late time point of 8 days could thus be involved in the long-term retraction of astrocytic endfeet 8 days after LPS administration observed in our model and could be the cause of the observed enwrapment of blood vessels by microglia [25].

These results are interesting as they demonstrate that astrocytes and microglia act synergistically to safeguard blood vessel coverage following neuroinflammation, suggesting that they both contribute to the maintenance of BBB integrity. However, they also reveal that each glial cell type

exhibits different kinetics of response to neuroinflammation resulting in a different duration pattern of vasculature coverage. The more transient response of microglia, which replaces loss of astrocytic coverage for a short period of time, may be one of the reasons contributing to the documented BBB leakage in severe neurodegenerative / neuroinflammatory conditions [29,30]. Collectively our findings come in accordance with recent studies supporting the role of reactive astrocytes as critical cellular mediators of vascular integrity after neuroinflammation [30] and implying their possible dynamic crosstalk with microglia in maintaning BBB integrity. Previous research has described joint regulatory activity of microglia and astrocytes, including cytokine secretion to adjust neuroinflammatory responses [21]. These cells also synergistically regulate blood vessel coverage dynamics, impacting NVU function and brain homeostasis. Further study into the role of reactive perivascular astrocytes and microglia within the frame of the complex NVU cellular system, under neuroinflammatory conditions is warranted.

Supplementary Materials: The following supporting information can be downloaded at the website of this paper posted on Preprints.org. Videos S1-S3: 3D reconstruction of a microglial cell in control mice (Video S1), 4 days (Video S2) and 8 days (Video S3) following LPS administration; Videos S4-S6: 3D reconstruction of an astrocyte in control mice (Video S4), 4 days (Video S2) and 8 days (Video S3) following LPS administration.

Author Contributions: EX, PNK and DT conceived project, designed experiments and analyzed and interpreted data; EX conducted intravital imaging experiments, confocal imaging and image analysis; PNK performed cranial window surgery and intravital imaging experiments; IT and MM performed in vivo experiments and immunohistochemistry; AS and FK provided transgenic mice and contributed in 2P intravital imaging setup; MSP, J-YT and EX developed image analysis tools and performed image analysis; EX and DT wrote the manuscript; DT supervised the project and acquired funding.

Funding: This work was financially supported by: 'BIOIMAGING-GR (MIS 5002755)', co-financed by Greece and EU Regional Development Fund; ARISTEIA-II 'Astro-Rep' 3713 Grant of the Greek Ministry of Education and International Pasteur Network Grant PTR-MIAD, awarded to DT. We also acknowledge funding from Stavros Niarhos Foundation to Hellenic Pasteur Institute, as part of the Foundation's initiative to support the Greek Research Center Ecosystem; Greek 'Flagship Action for the Study of Neurodegenerative Diseases on the Basis of Precision Medicine' and 'KRIPIS-II' Action (MIS 5002486).

Institutional Review Board Statement: The study was carried out in strict compliance with the European Directive 2010/63/EU and the Greek National Law 161/91 for Use of Laboratory Animals, according to FELASA recommendations for euthanasia and the National Institutes of Health Guide for Care and Use of Laboratory Animals. All protocols were approved by the Animal Care and Use Committee of the Hellenic Pasteur Institute (Animal House Establishment Code: EL 25 BIO 013). License No 490191/15-6-2021 for the experiments was issued by the Greek authorities of the Veterinary Department of the Athens Prefecture. The manuscript was prepared in compliance with the ARRIVE guidelines for reporting animal research.

Data Availability Statement: Fiji macros and notebooks for the entire image analysis pipeline are available at the public code hosting website: https://gitlab.pasteur.fr/iah-public/ptrmiad-mimika

Acknowledgments: We thank Prof. Bogdan Cătălin for extensive training in cranial window surgery and two photon imaging of living animals. We also thank Ioanna Giagklissi for assistance in establishing the LPS administration protocol.

Conflicts of Interest: The authors declare no conflict of interest.

References

1. B. C. Avendaño, T. D. Montero, C. E. Chávez, R. von Bernhardi, and J. A. Orellana, "Prenatal exposure to inflammatory conditions increases Cx43 and Panx1 unopposed channel opening and activation of astrocytes in the offspring effect on neuronal survival," *Glia*, vol. 63, no. 11, 2015, doi: 10.1002/glia.22877.
2. N. J. Abbott, L. Rönnbäck, and E. Hansson, "Astrocyte-endothelial interactions at the blood-brain barrier," *Nature Reviews Neuroscience*, vol. 7, no. 1. 2006. doi: 10.1038/nrn1824.
3. N. J. Abbott, A. A. K. Patabendige, D. E. M. Dolman, S. R. Yusof, and D. J. Begley, "Structure and function of the blood-brain barrier," *Neurobiol. Dis.*, vol. 37, no. 1, pp. 13–25, 2010, doi: 10.1016/j.nbd.2009.07.030.
4. J. Niu *et al.*, "HHS Public Access," vol. 22, no. 5, pp. 709–718, 2019, doi: 10.1038/s41593-019-0369-4.Aberrant.

5. G. Rajkowska, J. Hughes, C. A. Stockmeier, J. Javier Miguel-Hidalgo, and D. Maciag, "Coverage of blood vessels by astrocytic endfeet is reduced in major depressive disorder," *Biol. Psychiatry*, vol. 73, no. 7, pp. 613–621, 2013, doi: 10.1016/j.biopsych.2012.09.024.
6. E. Steiner *et al.*, "Loss of astrocyte polarization upon transient focal brain ischemia as a possible mechanism to counteract early edema formation," *Glia*, vol. 60, no. 11, pp. 1646–1659, 2012, doi: 10.1002/glia.22383.
7. N. Lou, T. Takano, Y. Pei, A. L. Xavier, S. A. Goldman, and M. Nedergaard, "Purinergic receptor P2RY12-dependent microglial closure of the injured blood-brain barrier," *Proc. Natl. Acad. Sci. U. S. A.*, vol. 113, no. 4, pp. 1074–1079, 2016, doi: 10.1073/pnas.1520398113.
8. F. Helmchen and W. Denk, "Deep tissue two-photon microscopy," *Nat. Methods*, vol. 2, no. 12, pp. 932–940, 2005, doi: 10.1038/nmeth818.
9. D. Davalos *et al.*, "Stable in vivo imaging of densely populated glia, axons and blood vessels in the mouse spinal cord using two-photon microscopy," *J. Neurosci. Methods*, vol. 169, no. 1, pp. 1–7, 2008, doi: 10.1016/j.jneumeth.2007.11.011.
10. C. R. A. Batista, G. F. Gomes, E. Candelario-Jalil, B. L. Fiebich, and A. C. P. de Oliveira, "Lipopolysaccharide-induced neuroinflammation as a bridge to understand neurodegeneration," *Int. J. Mol. Sci.*, vol. 20, no. 9, 2019, doi: 10.3390/ijms20092293.
11. S. Jung *et al.*, " Analysis of Fractalkine Receptor CX 3 CR1 Function by Targeted Deletion and Green Fluorescent Protein Reporter Gene Insertion ," *Mol. Cell. Biol.*, vol. 20, no. 11, pp. 4106–4114, 2000, doi: 10.1128/mcb.20.11.4106-4114.2000.
12. P. G. Hirrlinger *et al.*, "Expression of reef coral fluorescent proteins in the central nervous system of transgenic mice," *Mol. Cell. Neurosci.*, vol. 30, no. 3, 2005, doi: 10.1016/j.mcn.2005.08.011.
13. J. Schindelin *et al.*, "Fiji: An open-source platform for biological-image analysis," *Nature Methods*, vol. 9, no. 7. pp. 676–682, 2012. doi: 10.1038/nmeth.2019.
14. T. Kluyver *et al.*, "Jupyter Notebooks—a publishing format for reproducible computational workflows," in *Positioning and Power in Academic Publishing: Players, Agents and Agendas - Proceedings of the 20th International Conference on Electronic Publishing, ELPUB 2016*, 2016, pp. 87–90. doi: 10.3233/978-1-61499-649-1-87.
15. J. N. Kapur, P. K. Sahoo, and A. K. C. Wong, "A new method for gray-level picture thresholding using the entropy of the histogram.," *Comput. Vision, Graph. Image Process.*, vol. 29, no. 3, pp. 273–285, 1985, doi: 10.1016/0734-189X(85)90125-2.
16. D. Legland, I. Arganda-Carreras, and P. Andrey, "MorphoLibJ: Integrated library and plugins for mathematical morphology with ImageJ," *Bioinformatics*, vol. 32, no. 22, pp. 3532–3534, 2016, doi: 10.1093/bioinformatics/btw413.
17. N. Otsu, "THRESHOLD SELECTION METHOD FROM GRAY-LEVEL HISTOGRAMS.," *IEEE Trans Syst Man Cybern*, vol. SMC-9, no. 1, pp. 62–66, 1979, doi: 10.1109/tsmc.1979.4310076.
18. E. A. Nagelhus *et al.*, "Aquaporin-4 water channel protein in the rat retina and optic nerve: Polarized expression in Muller cells and fibrous astrocytes," *J. Neurosci.*, vol. 18, no. 7, pp. 2506–2519, 1998, doi: 10.1523/jneurosci.18-07-02506.1998.
19. S. Gyoneva *et al.*, "Systemic inflammation regulates microglial responses to tissue damage in vivo," *Glia*, vol. 62, no. 8, pp. 1345–1360, 2014, doi: 10.1002/glia.22686.
20. P. Hasel, I. V. L. Rose, J. S. Sadick, R. D. Kim, and S. A. Liddelow, "Neuroinflammatory astrocyte subtypes in the mouse brain," *Nat. Neurosci.*, vol. 24, no. 10, pp. 1475–1487, 2021, doi: 10.1038/s41593-021-00905-6.
21. S. A. Liddelow *et al.*, "Neurotoxic reactive astrocytes are induced by activated microglia," *Nature*, vol. 541, no. 7638, pp. 481–487, 2017, doi: 10.1038/nature21029.
22. H. Kubotera, H. Ikeshima-Kataoka, Y. Hatashita, A. L. Allegra Mascaro, F. S. Pavone, and T. Inoue, "Astrocytic endfeet re-cover blood vessels after removal by laser ablation," *Sci. Rep.*, vol. 9, no. 1, pp. 1–10, 2019, doi: 10.1038/s41598-018-37419-4.
23. B. P. Heithoff, K. K. George, A. N. Phares, I. A. Zuidhoek, C. Munoz-Ballester, and S. Robel, "Astrocytes are necessary for blood–brain barrier maintenance in the adult mouse brain," *Glia*, vol. 69, no. 2, pp. 436–472, 2021, doi: 10.1002/glia.23908.
24. W. A. Mills *et al.*, "Astrocyte plasticity in mice ensures continued endfoot coverage of cerebral blood vessels following injury and declines with age," *Nat. Commun.*, vol. 13, no. 1, pp. 1–15, 2022, doi: 10.1038/s41467-022-29475-2.
25. E. Mondo *et al.*, "A developmental analysis of juxtavascular microglia dynamics and interactions with the vasculature," *J. Neurosci.*, 2020, doi: 10.1523/JNEUROSCI.3006-19.2020.
26. K. Haruwaka *et al.*, "Dual microglia effects on blood brain barrier permeability induced by systemic inflammation," *Nat. Commun.*, vol. 10, no. 1, pp. 1–17, 2019, doi: 10.1038/s41467-019-13812-z.
27. A. M. Fukuda and J. Badaut, "Aquaporin 4: A player in cerebral edema and neuroinflammation," *J. Neuroinflammation*, vol. 9, no. 1, p. 1, 2012, doi: 10.1186/1742-2094-9-279.
28. B. Di Benedetto *et al.*, "Fluoxetine requires the endfeet protein aquaporin-4 to enhance plasticity of astrocyte processes," *Front. Cell. Neurosci.*, vol. 10, no. FEB, 2016, doi: 10.3389/fncel.2016.00008.

 doi:10.20944/preprints202303.0525.v1

29. T. G. Bush *et al.*, "Leukocyte Infiltration, Neuronal Degeneration, and Neurite Outgrowth after Ablation of Scar-Forming, Reactive Astrocytes in Adult Transgenic Mice provision of metabolic substrates for neurons, and inter-actions with endothelia to create and maintain the b," *Neuron*, vol. 23, pp. 297–308, 1999.
30. M. R. Williamson, C. J. A. Fuertes, A. K. Dunn, M. R. Drew, and T. A. Jones, "Reactive astrocytes facilitate vascular repair and remodeling after stroke," *Cell Rep.*, vol. 35, no. 4, p. 109048, 2021, doi: 10.1016/j.celrep.2021.109048.